

RADARSAT ScanSAR Wind Retrieval Under Hurricane Conditions

Congling Nie and David G. Long Department of Electrical and Computer Engineering,
Brigham Young University, Provo, Utah
Phone:801-422-4884 Email:nie@mers.byu.edu

ABSTRACT

RADARSAT-1 ScanSAR SWA images of Hurricane Katrina are used to retrieve the surface wind vectors over the ocean. Due to the inadequate spatial resolution of the ScanSAR SWA images, the spectrum method cannot be implemented to estimate the wind direction. Instead, collocated H*wind wind directions are used as wind direction estimates. The wind speed is derived from the σ° by inversion of a C-band HH-polarization Geophysical Model Function (GMF), which is derived from C-band VV-polarization GMF using a polarization ratio model. Because existing polarization models don't fit the ScanSAR SWA data well, a recalibration model is proposed to "recalibrate" the ScanSAR SWA images. The coefficients of the recalibration model are "tuned" using collocated H*wind surface wind fields. To validate the SAR-retrieved wind speed, the mean and the RMS difference between SAR-retrieved and H*wind wind speed estimates are calculated. The mean of difference is small and the RMS for wind speed less than 25 m/s is below 4 m/s, suggesting that the high resolution wind retrieval algorithm can work under hurricane conditions. Except for the influence from rain, the largest errors occur at high wind speed (over 25 m/s), which is mainly due to the saturation of the C-band GMF CMOD5.

1. INTRODUCTION

Synthetic aperture radar (SAR) has been used to study coastal processes, currents, and sea ice with its high spatial resolution and large spatial coverage. In recent years, vector winds over the ocean have been retrieved from SAR images. Similar to scatterometry, the normalized radar cross section (σ°) measured by SAR over the ocean is mainly from wind-driven gravity-capillary waves (Bragg waves). σ° is related to wind velocity and wind direction through an empirical model, known as the Geophysical Model Function (GMF). Since SAR has only one measurement for each geographic location, wind speed and direction can not be retrieved by direct inversion of the GMF. The wind direction can be estimated by measuring the orientation of the wind-induced streaks visible in most SAR images^{1,2,3} or obtained from additional information such as numerical wind prediction. For wind speed retrieval, there are two main methods. One of them estimates wind speed from the spectral width of the image spectrum in azimuth direction. The other one estimates wind speed by inversion of the GMF with input of the σ° , incidence angle, azimuth angle, and wind direction.

The Canadian satellite RADARSAT-1 works at 5.3 GHz(C-band) in HH polarization. The scanning SAR (ScanSAR) wide (SWA) mode of RADARSAT-1 provides coverage of a 500km nominal ground swaths at incidence angles between 20 and 49 degrees, with a spatial resolution of 100 m.⁴ Because ScanSAR SWA's resolution is insufficient to implement the spectrum method for wind speed estimation, wind speed must be estimated by inversion of GMF. There is no well-validated GMF model for HH polarization at C-band. General approach to obtain a HH polarization GMF is adjusting C-band VV polarization GMF (CMOD) using a polarization ratio p . While several C-band polarization ratio models have been proposed, none has been well verified.

Although different SAR images have been used to retrieve vector winds over the ocean. SAR wind retrieval for hurricanes has not been carefully studied. In this study, ScanSAR SWA images acquired during the period of hurricane Katrina are recalibrated and wind retrieval method are performed to estimate the surface winds over the ocean. In the next section, details of the data set used in the study are described. The principles of SAR wind retrieval are illustrated in section III, while the retrieval results are analyzed and validated in section IV.

2. DATA

Two 510 km \times 510 km calibrated RADARSAT-1 ScanSAR SWA images acquired over the ocean around New Orleans on 23:49:05 and 23:50:50, 28 August, 2005, during the period of Hurricane Katrina, are used to retrieve the vector winds. At the time of observation, the hurricane was a category 5 hurricane with a fully developed eye.

RADARSAT-1 was launched in 1994 for environmental monitoring. The satellite operates on a sun synchronous dawn-dusk orbit at an nominal altitude of 793 to 821 km.⁴ Among the different working modes of RADARSAT-1, the ScanSAR

wide A (SWA) mode allows imaging of the widest swath of about 500 km, which is ideal for monitoring hurricanes. SWA has a range of incidence angles between 20 to 49 degrees. To create SWA product, RADARSAT combines four beams (W1, W2, W3, and S7) during data collection, with each beam scanned sequentially. The nominal image coverage of ScanSAR SWA is 500 km \times 500 km, while the image processed by Alaska Satellite Facility (ASF) is 510 km \times 510 km with a pixel spacing of 50 m. The range resolution of the four beams varies from 73.3 m to 162.7 m, while the azimuth resolution varies from 93.1 m to 117.5 m. The raw ScanSAR SWA data were processed by the ASF into calibrated images. However, the radiometric calibration of ScanSAR SWA images is very difficult due to many limitations. Because of incorrect radiometric compensation for the azimuth antenna pattern, non-zeros yaw steering, and inaccurate center Doppler frequency, scalloping may occur in specific areas. Furthermore, saturation of the analog to digital converter (ADC) leads to an underestimation of σ° .⁵ Beam overlap regions can occur due to incorrect radiometric compensation for the range antenna pattern and roll angle ambiguity. It is also noted that the calibration at ASF is mainly “tuned” to the high latitude areas, which may result in degraded calibration for low latitude areas. The accuracy of the ASF calibrated SWA images has not been well studied. In,⁶ the relative radiometric accuracy for SWA is estimated to be about 0.47dB. The geographic location accuracy of the ScanSAR SWA images is still not available, while the overall relative location error for a similar product, ScanSAR SWB, is about 135 m.

To retrieve the vector winds, parameters needed for wind retrieval process are estimated from the SAR image. The incidence angle for each image pixel is calculated from ScanSAR SWA data with a method proposed in.⁷ Because the format of ASF processed ScanSAR SWA data is not the same as CDPF products, the normalized radar cross section σ° is calculated from the digital number (DN) of each pixel by

$$\sigma^\circ = 10\log_{10}[(DN_j^2 + A3)/A2_j] \text{ dB} \quad (1)$$

where $A2_j$ is the scaling gain value for the j th pixel, and $A3$ is the fixed offset to compensate for the noise floor. Since information is unavailable to calculate a nominal noise vector for ScanSAR SWA product, the $A3$ is set to 0 for all ASF calibrated ScanSAR SWA products.

To validate the SAR retrieved wind fields, coincident H*wind surface wind fields⁸ are used in the study. The H*wind Surface Wind Analysis System is a high resolution hurricane research tool for assimilating and synthesizing disparate observations into a consistent wind field. H*wind uses all available surface weather observations including NOAA P3 and G4 research aircraft measured data, retrieved winds from SSM/I, ERS, QuikScat, and TRMM, and GOES cloud drift winds to predict surface wind fields. All data are processed to conform to a common framework for 10 m height, the same exposure, and the same averaging period using accepted methods from micrometeorology and wind engineering.⁹ The spatial resolution of H*wind wind estimate is 0.0542 degree in latitude and longitude, while the time resolution is 3 hours.

3. SAR WIND RETRIEVAL

As mentioned in section II, the wind direction can be derived from the orientation of wind-induced streaks, such as boundary layer rolls in the atmosphere, which are visible in many SAR images. In such images the spectrum method can be implemented to estimate the wind direction. However this method has not proved applicable to these RADARSAT-1 ScanSAR images, due to the inadequate spatial resolution of the images.⁵ Therefore, additional information such as numerical predicted wind fields must be used to estimate of the wind direction. For a hurricane, the wind direction can also be estimated by combining the SAR images with hurricane dynamic models. In the study, the collocated H*wind wind direction field is used as the wind direction estimates.

Knowing the wind direction, the wind speed can be derived from the σ° by inversion of the GMF with input of the incidence angle θ , and the azimuth angle, and the wind directions. Lacking a well-validated GMF for C-band HH polarization, the GMF for C-band VV polarization is modified using the C-band polarization ratio to estimate the σ° . The polarization ratio p is defined as

$$p = \frac{\sigma_{HH}^\circ}{\sigma_{VV}^\circ} \quad (2)$$

where σ_{HH}° and σ_{VV}° are the σ° in HH and VV polarization, respectively. The polarization ratio is less than one for moderate incidence angles (20° to 70°). For C-band, polarization ratio p is dependent on the incidence angle.¹⁰ For low

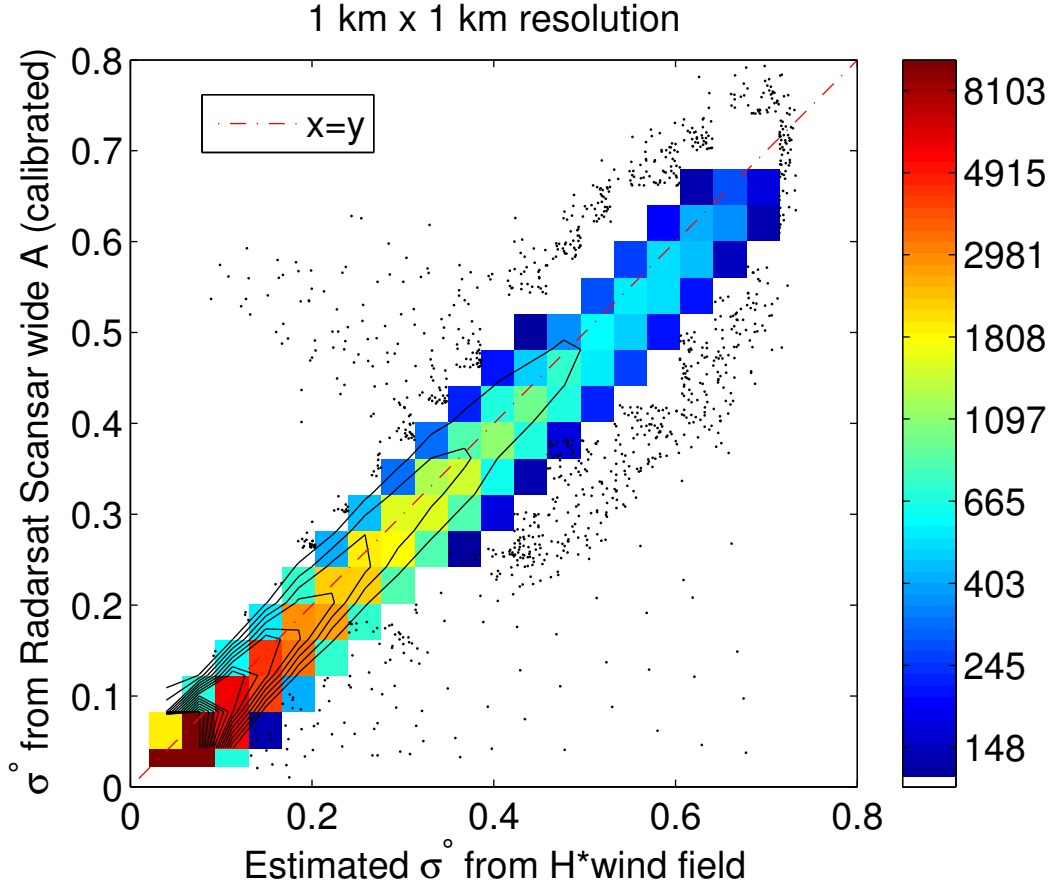


Figure 1. Scatter density plot between the σ° of re-calibrated SAR image A and σ° estimated from collocated H*wind. Both σ° axes are in normal space. The resolution of σ° is $1 \text{ km} \times 1 \text{ km}$.

wind speed, p has some dependency on wind speed, while the variation of p with wind speed is quite small for medium to high wind speeds. A wind direction dependency is also observed by Mouche et al.¹¹ for the incidence angle of 45° . Several C-band polarization models have been proposed using different data sets. Thompson et al.¹² developed a model for the polarization ratio with incidence angle

$$p = \frac{(1 + \alpha \tan^2 \theta)^2}{(1 + 2 \tan^2 \theta)^2} \quad (3)$$

where θ is the incidence angle, and α is a constant. The value of α is determined as 0.6 by fitting the model to the data measured with an airborne SCAT by Unal et al.¹⁰ for several moderate incidence angles with low to medium wind speeds. The $\alpha = 0.6$ ensures that the proposed model is consistent with both the theoretical polarization ratio for Bragg scattering with $\alpha = 0$ and the Kirchhoff scattering with $\alpha = 2$. The $\alpha = 0.6$ is verified by Monaldo et al.^{13,14} using RADARSAT-1 data and in situ data, while Vachon and Dbozon¹ found that using Thompson's model with $\alpha = 0.6$ leads to a wind speed overestimate, especially for high wind speeds. The value of α recommended by their study is 1.

Another model was proposed by Elfouhaily¹⁵

$$p = \frac{(1 + 2 \sin^2 \theta)^2}{(1 + 2 \tan^2 \theta)^2} \quad (4)$$

The model was obtained by transforming the effective scattering Fresnel coefficient of vertical polarization to horizontal polarization. Using dual-polarization measurements from airborne radar observations, Mouche et al.¹⁶ proposed an

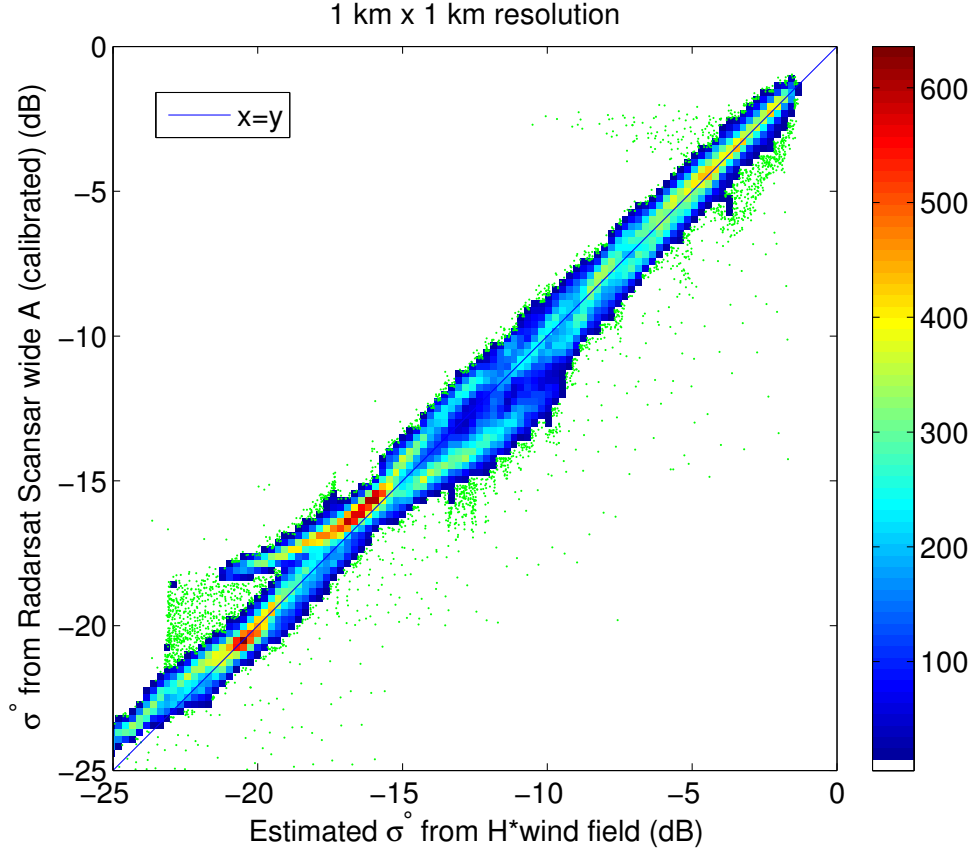


Figure 2. Scatter density plot between the σ° of re-calibrated SAR image A and σ° estimated from collocated H*wind. Both σ° axes are in log space.

empirical model

$$p = Ae^{B\theta} + C. \quad (5)$$

where $A = 0.008$, $B = 0.1255$, and $C = 0.9973$.

Because each of the models mentioned above is not well-validated and the model coefficients have dependency on the specific data set, we compared different models using our data and “tuned” the model coefficients for optimum performance. The σ° estimates from SAR image DN values are compared with the σ° estimated using H*wind wind estimates projected through CMOD5 and the polarization model. It is found that the Thompson’s model fits image A relatively well, which was acquired on 23:49:05, while the other two models both underestimate the σ° . But all three models do not fit image B well, which was acquired on 23:50:50. Image B was acquired over the transition area between ocean and land, which may be the reason for the degraded calibration. Thus, we adopt a method proposed in¹⁷ to recalibrate the SAR images. The model coefficients are “tuned” for optimum performance using collocated H*wind wind fields projected through CMOD5 and Thompson’s polarization model. The re-calibrated σ_{re}° can be expressed as

$$\sigma_{re}^\circ = \sigma_{es}^\circ G(\theta)M + O \quad (6)$$

where σ_{es}° is the σ° estimates from DN value using equation (1), $G(\theta)$ is a parameter dependent on incidence angle, M is a power correction parameter, and O is an offset correction parameter. $G(\theta)$ can be expressed as

$$G(\theta) = \sin^n(\theta) \quad (7)$$

where n is a real number. Since ScanSAR SWA combines data from four different beams, each with different incidence angles and different radiometric characteristics, the coefficients of the recalibration model are separately “tuned” for each

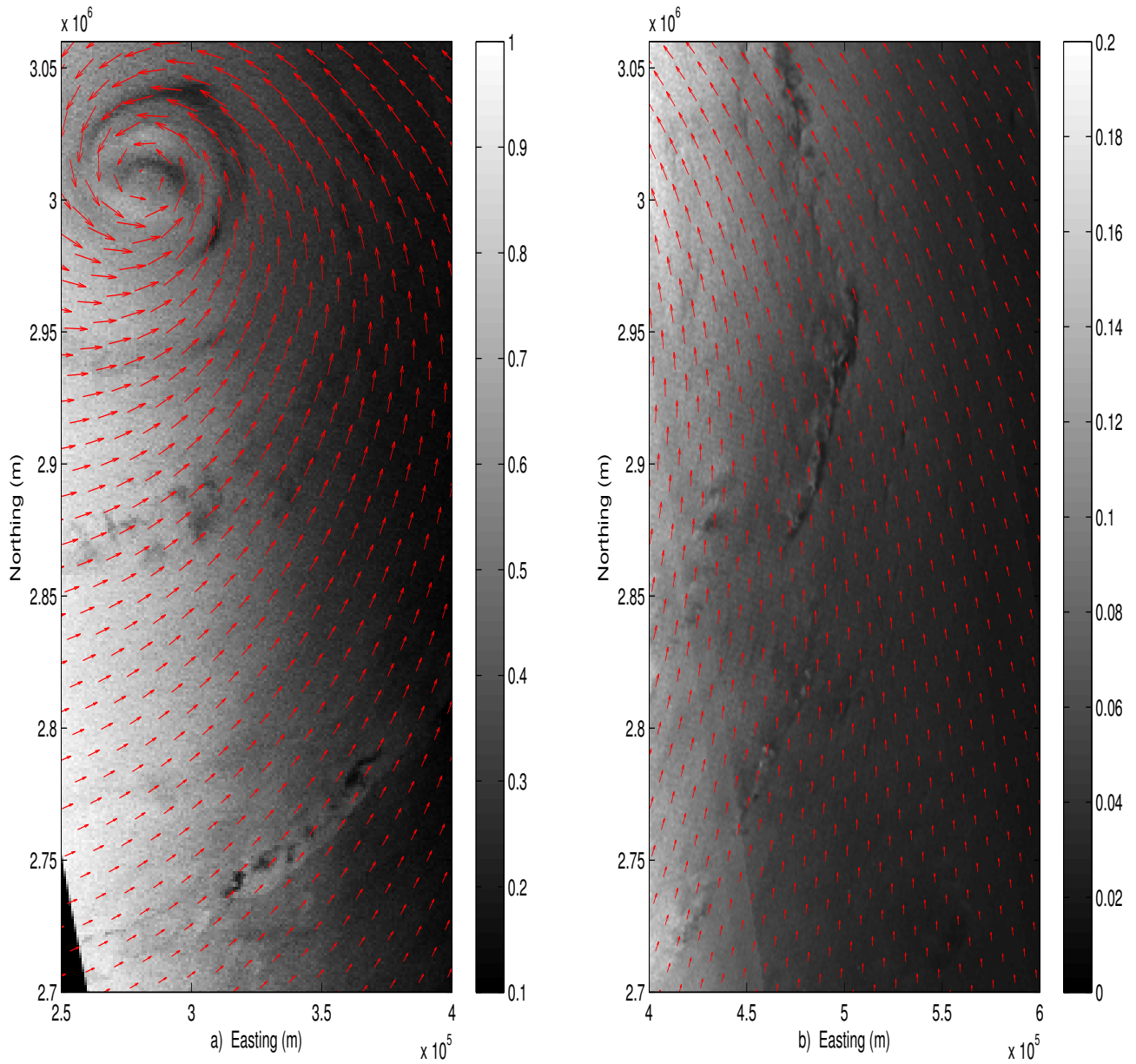


Figure 3. Two selected areas for SAR image A. σ° is plotted with collocated H*wind direction field. The resolution of σ° is $1 \text{ km} \times 1 \text{ km}$. The resolution of H*wind wind vectors is about $10 \text{ km} \times 10 \text{ km}$. Due to decreasing of incidence angles from left to right, the σ° changes from light to dark. Because of “recalibration”, artificial panels can be observed along the azimuth direction. Rain bands are visible in both panels. Noted that the color-maps of a) and b) are different.

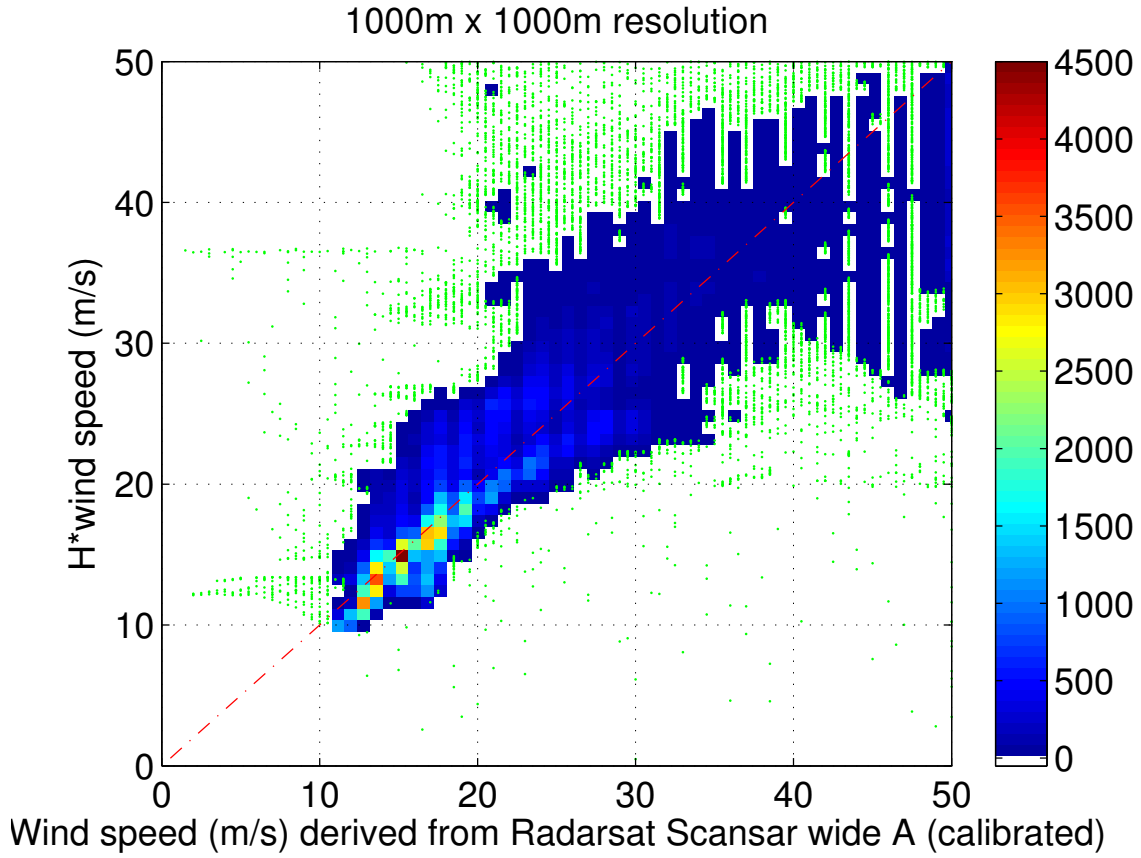


Figure 4. Scatter density plot for the SAR-derived wind speed and H*wind speed for SAR image A in (m/s).

of the three incidence angle ranges. Table 1 shows the recalibration coefficients for three incidence angle bins of 22-31 degrees, 31-41 degrees, and 41-47 degrees respectively. The scatter plots between the two σ° estimates in normal space and log-log space for image A are shown in Figs. 1 and 2. It is noted that except for incidence angle range 22-31 degrees, the coefficients of the recalibration model are very close, showing the recalibration model is consistent for different SAR image segments.

Table 1. Coefficients of the recalibration model

Image name	incidence angle (degree)	n	M	O
A	22 - 31	-1.12	0.34	0.032
B	22 - 31	-1.7	0.22	0.002
A	31 - 41	-1.2	0.32	0.01
B	31 - 41	-1.18	0.27	0.008
A	41 - 47	-1.11	0.33	0.003
B	41 - 47	-1.115	0.33	0.0055

4. WIND RETRIEVAL RESULTS AND ANALYSIS

In this section, the vector winds retrieved from the two ScanSAR SWA images are presented. Wind retrieval is done at $1 \text{ km} \times 1 \text{ km}$ by inversion of the GMF using recalibrated σ° . In Fig. 3, portions of both re-calibrated σ° and collocated H*wind wind direction vectors of image A are shown. Since the magnitude range of σ° is big, we display σ° of image A in two sub-images. It is noted that the color-map of sub-image a) and b) are different. Visually, the H*wind wind directions

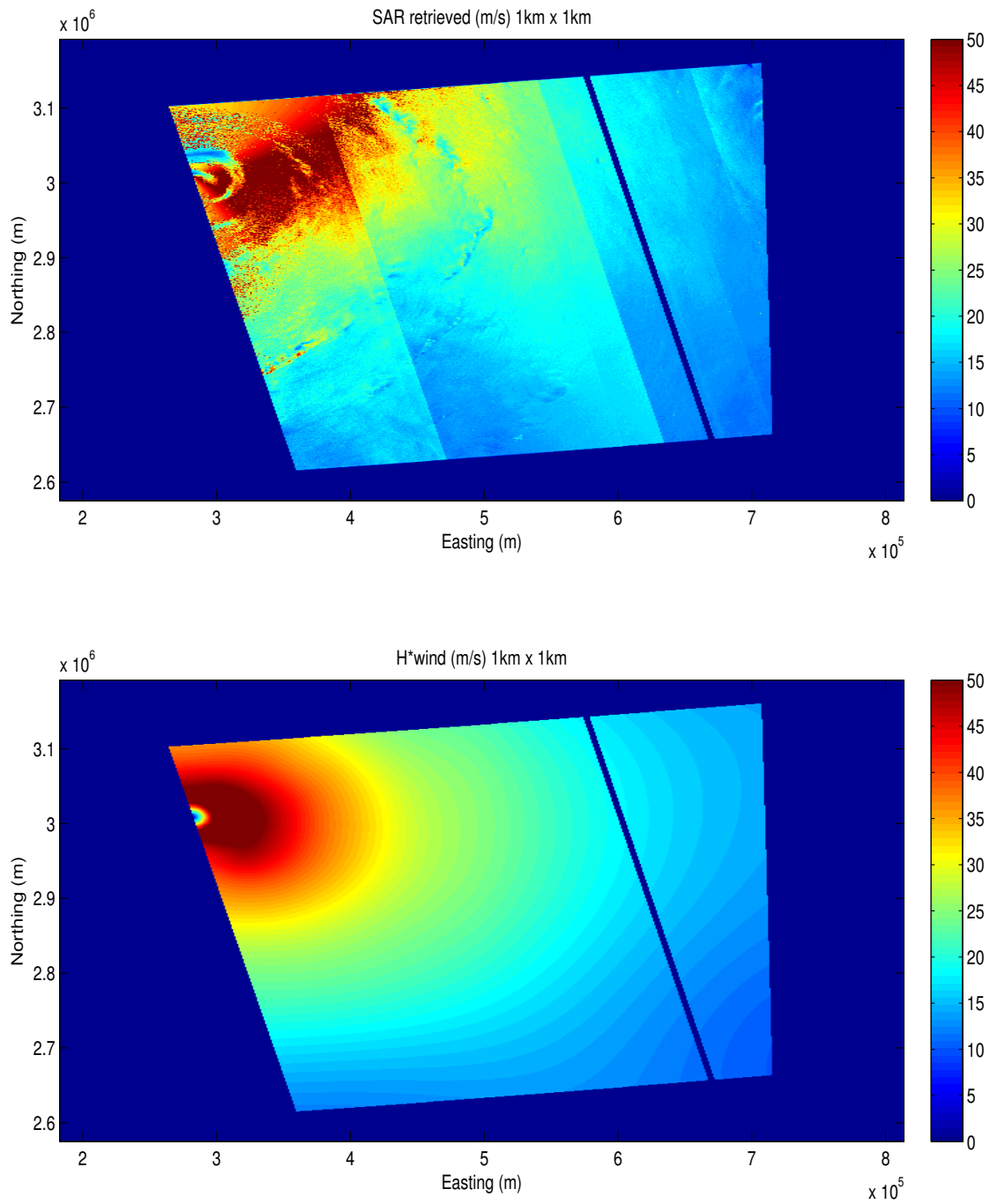


Figure 5. Comparison between SAR derived wind speed (top) and H*wind speed (bottom) for SAR image A in (m/s). Due to “recalibration”, artificial panels can be observed along the azimuth direction. Wind speeds are possibly overestimated in an area near the eye wall at about northing $3.08E6$ m and easting $4.5E5$ m. A dark stripe along the track is due to elimination of invalid data.

agree well with the key features in the SAR image. Since the magnitude of σ° decreases with increasing incidence angle for a specific wind speed and direction, pixels generally become darker from left to right, since incidence angle decreases from left to right. Rain bands and rain cells are visible in σ° field. For the C-band SAR signal, the effects of rain on σ° vary with incidence angle. At high incidence angles, rain generally enhances the backscatter, while rain reduces the backscatter at low incidence angles. At moderate incidence angles, the effect of rain is complex. In Fig. 3, we can observe dark spiral rain bands around the hurricane eye, which is due to diminution of σ° by rain. While rain adversely affects the wind accuracy, it is not considered in the wind retrieval.

To validate the SAR-derived wind speeds, we show scatter density plots between the SAR retrieved wind speed fields and the collocated H*wind wind speed fields for image A in Fig. 4. Overall, SAR-derived wind speeds agree well with H*wind wind speeds. Except for the influence from rain, the largest errors of wind speed occur at high wind speed (over 25 m/s), where the SAR-derived wind speeds have considerable scatter in comparison to the H*wind wind speeds. These errors are mainly due to the saturation of the C-band GMF CMOD5. Another possible reason is inaccuracy of CMOD5 for high wind speed. As shown in Fig. 6, the shape of σ° as a function of wind speed becomes flat over 25 m/s. As a result, the wind retrieval becomes very sensitive to noise for high wind speed and variability of the wind estimates is increased. We show the compact comparison between the two wind speed estimates for image A in Fig. 5. As mentioned above, the SAR-retrieved wind speed is noisier in high wind areas (near the hurricane eye). Wind speeds are possibly overestimated in an area near the eye wall at about northing 3.08E6 m and easting 4.5E5 m. Due to “recalibration”, artificial panels can be observed along the azimuth direction. Effects of rain are also noticeable in the SAR-retrieved wind speed field.

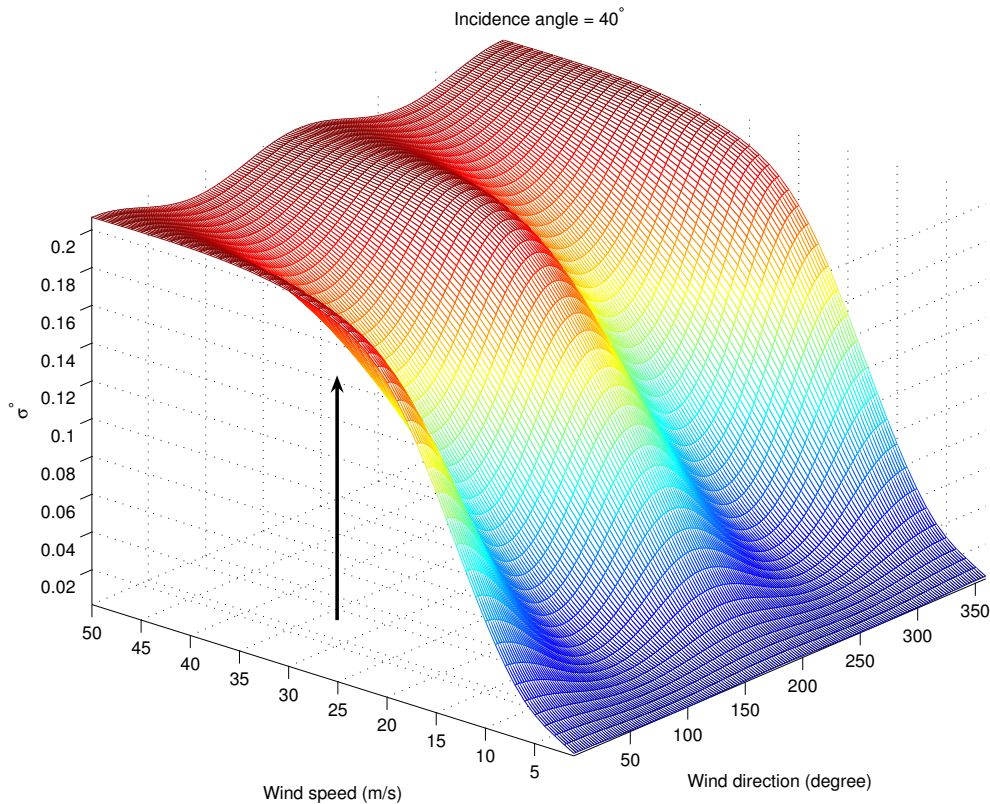


Figure 6. CMOD5 GMF as a function of wind speed and wind direction for incidence angle 40°. GMF becomes flat for wind speed over 25 m/s.

The mean of error (SAR retrieved wind speed - H*wind wind speed) and RMS between the two wind speed estimates are listed in Table 2. The ScanSAR SWA retrieved wind speeds has a small bias, which is possibly caused by rain contamination. The overall root mean squared error (RMS) is below 6 m/s and RMS for wind speed less than 25 m/s is below

Table 2. Mean of error and RMS between the SAR retrieved wind speeds and H*wind wind speeds

Image	Mean of error (SAR estimated speed - H*wind speed) (m/s)	RMS (overall) (m/s)	RMS(<25 m/s) (m/s)
A	-0.21	4.53	2.5
B	0.38	5.7	3.5

4 m/s, demonstrating relatively high accuracy of SAR-retrieved wind speeds in hurricanes. Future analysis will include compensating for the effects of rain in the wind retrieval.

5. CONCLUSION

RADARSAT-1 ScanSAR SWA images are used to derive the wind speed under hurricane conditions. A recalibration model has been proposed to adjust the ASF calibrated ScanSAR SWA images. The SAR retrieved wind speeds agree well with the collocated H*wind wind speeds, though large errors occur for high wind speed due to the saturation of GMF. Bias between the two wind speed estimates is negligible and the RMS is relatively small, showing the RADARSAT-1 ScanSAR SWA images processed by the recalibration model are capable of being used to derive ocean surface winds in hurricanes.

REFERENCES

1. P. W. Vachon and F. W. Dobson, Validation of wind vector retrieval from ERS-1 SAR images over the ocean, *Global Atmos. Ocean Syst.*, vol. 5, pp 177-187, 1996.
2. C. C. Wackerman, C. L. Rufenach, R. Schuchman, J. A. Johnnessen, and K. Davidson, Wind vector retrieval using ERS-1 synthetic aperture radar imagery, *J. Geophys. Res.*, vol. 34, pp. 1343-1352, 1996.
3. S. Lehner, J. Horstmann, W. Koch, and W. Rosenthal, Mesoscale wind measurements using recalibrated ERS SAR images, *J. Geophys. Res.*, vol. 103, pp. 7847-7856, 1998.
4. R. K. Raney, A. P. Luscombe, E. J. Langham, S. Ahmed, Radarsat, *Proceedings IEEE*, vol. 79, pp. 839-849, 1991.
5. J. Horstmann, W. Koch, S. Lehner, and R. Tonboe, Wind retrieval over the ocean using synthetic aperture radar with C-band HH polarization, *IEEE Trans. Geosci. Remote Sens.*, vol. 38, No.5, 2000.
6. W. Albright, Calibration report for RADARSAT ScanSAR wind A on the ScanSAR processor, Alaska SAR facility, 2004.
7. N. Shepherd, Extraction of beta nought and sigma nought from RADARSAT CDPF products, Rep. AS97 - 5001 Rev. 2, Can. Space Agency, Ottawa, ON, Canada, 1998.
8. M. D. Powell, S.H. Houston, L.R. Amat, and N. Morisseau-Leroy, The HRD real-time hurricane wind analysis system, *J. Wind Engineer. and Indust. Aerodyn*, 77 - 78, pp. 53-64, 1998.
9. M. D. Powell, S.H. Houston, and T.A. Reinhold, Hurricane Andrew's landfall in South Florida Part I : Standardizing measurements for documentation of surface wind fields, *Wea. Forecast.* 11, pp. 304-328, 1996.
10. C. M. H. Unal, P. Snooji, and P. J. F. Swart, The polarization-dependent relation between radar backscatter from the ocean surface and surface wind vectors at frequencies between 1 and 18 GHz, *IEEE Trans. Geosci. Remote Sens.*, vol. 29, pp. 621-626, 1991.
11. A. A. Mouche, D. Hauser, J. F. Daloze, and C. Guerin, Dual-polarization measurements at C-band over the ocean: results from airborne radar observations and comparison with ENVISAT ASAR data, *IEEE Trans. Geos. Remote Sens.*, Vol. 43, No. 4, Apr. 2005.
12. D. R. Thompson, T. M. Elfouhaily, and B. Chapron, Polarization ratio from microwave backscattering from the ocean surface at low to moderate incidence angles, in Proc. Int. Geoscience and Remote Sensing Symp., 1998, Seattle, WA, 1998.
13. F. M. Monaldo, D. R. Thompson, R. C. Beal, W. G. Pichel, and P. Clemente-Colon, Comparison of SAR-Derived wind speed with model predictions and ocean buoy measurements, *IEEE Trans. Geosci. Remote Sens.*, vol. 39, no. 12, pp. 2587-2600, 2001.
14. F. M. monaldo, C. C. Wackerman and P. Clemente-Colon, A two scale model to predict C-band VV and HH normalized radar cross section values over the ocean, *Can. J. Remote Sens.*, vol. 28, no. 3, pp. 367-384, 2002.

15. T. Elfouhaily, Physical modeling of electromagnetic backscatter from the ocean surface; Application to retrieval of wind fields and wind stress by remote sensing of the marine atmospheric boundary layer, *Ph.D dissertation*, Dpt. d'Océanogr. Spatiale, Inst.Franais Rec.(IFREMER), Plouzane, France, 1997.
16. A. A. Mouche, D. Hauser, J. F. Daloze, and C. Guerin, Dual-polarization measurements at C-band over the ocean: results from airborne radar observations and comparison with ENVISAT ASAR data, *IEEE Trans. Geosci.Remote Sens.* Vol. 43, No. 4, 2005.
17. J. Gower and S. Skey, Wind, slick, and fishing boat observations with Radarsat ScanSAR, *Johns Hopkins APL Technical Digest*, vol. 21, No. 1, 2000.